doi:10.1093/brain/aww229 BRAIN 2016: 139; 3151–3162 | 3151

BRAIN
A JOURNAL OF NEUROLOGY

Microbleed and microinfarct detection in amyloid angiopathy: a high-resolution MRI-histopathology study

Susanne J. van Veluw,[1,2] Andreas Charidimou,[1] Andre J. van der Kouwe,[3] Arne Lauer,[1] Yael D. Reijmer,[1] Isabel Costantino,[4] M. Edip Gurol,[1] Geert Jan Biessels,[2] Matthew P. Frosch,[4] Anand Viswanathan[1] and Steven M. Greenberg[1]

Cerebral amyloid angiopathy is a common neuropathological finding in the ageing human brain, associated with cognitive impairment. Neuroimaging markers of severe cerebral amyloid angiopathy are cortical microbleeds and microinfarcts. These parenchymal brain lesions are considered key contributors to cognitive impairment. Therefore, they are important targets for therapeutic strategies and may serve as surrogate neuroimaging markers in clinical trials. We aimed to gain more insight into the pathological basis of magnetic resonance imaging-defined microbleeds and microinfarcts in cerebral amyloid angiopathy, and to explore the pathological burden that remains undetected, by using high and ultra-high resolution *ex vivo* magnetic resonance imaging, as well as detailed histological sampling. Brain samples from five cases (mean age 85 ± 6 years) with pathology-proven cerebral amyloid angiopathy and multiple microbleeds on *in vivo* clinical magnetic resonance imaging were subjected to high-resolution *ex vivo* 7 T magnetic resonance imaging. On the obtained high-resolution (200 µm isotropic voxels) *ex vivo* magnetic resonance images, 171 microbleeds were detected compared to 66 microbleeds on the corresponding *in vivo* magnetic resonance images. Of 13 sampled microbleeds that were matched on histology, five proved to be acute and eight old microhaemorrhages. The iron-positive old microhaemorrhages appeared approximately four times larger on magnetic resonance imaging compared to their size on histology. In addition, 48 microinfarcts were observed on *ex vivo* magnetic resonance imaging in three out of five cases (two cases exhibited no microinfarcts). None of them were visible on *in vivo* 1.5 T magnetic resonance imaging after a retrospective analysis. Of nine sampled microinfarcts that were matched on histology, five were confirmed as acute and four as old microinfarcts. Finally, we explored the proportion of microhaemorrhage and microinfarct burden that is beyond the detection limits of *ex vivo* magnetic resonance imaging, by scanning a smaller sample at ultra-high resolution, followed by serial sectioning. At ultra-high resolution (75 µm isotropic voxels) magnetic resonance imaging we observed an additional 48 microbleeds (compared to high resolution), which proved to correspond to vasculopathic changes (i.e. morphological changes to the small vessels) instead of frank haemorrhages on histology. After assessing the serial sections of this particular sample, no additional haemorrhages were observed that were missed on magnetic resonance imaging. In contrast, nine microinfarcts were found in these sections, of which six were only retrospectively visible at ultra-high resolution. In conclusion, these findings suggest that microbleeds on *in vivo* magnetic resonance imaging are specific for microhaemorrhages in cerebral amyloid angiopathy, and that increasing the resolution of magnetic resonance images results in the detection of more 'non-haemorrhagic' pathology. In contrast, the vast majority of microinfarcts currently remain under the detection limits of clinical *in vivo* magnetic resonance imaging.

1 J. Philip Kistler Stroke Research Center, Department of Neurology, Massachusetts General Hospital and Harvard Medical School, Boston, MA, USA
2 Department of Neurology, Brain Center Rudolf Magnus, University Medical Center Utrecht, Utrecht, The Netherlands
3 Athinoula A. Martinos Center for Biomedical Research, Department of Radiology, Massachusetts General Hospital and Harvard Medical School, Charlestown, MA, USA

Received March 18, 2016. Revised July 5, 2016. Accepted July 31, 2016. Advance Access publication September 19, 2016

4 Neuropathology Service, C.S. Kubik Laboratory for Neuropathology, Massachusetts General Hospital and Harvard Medical School, Boston, MA, USA

Correspondence to: Susanne J. van Veluw
J. Philip Kistler Stroke Research Center,
Department of Neurology, Massachusetts General Hospital,
175 Cambridge Street, Suite 300, Boston, MA 02114, USA
E-mail: svanveluw@mgh.harvard.edu

Keywords: small vessel disease; post-mortem MRI; histology; microbleeds; microinfarcts

Abbreviations: CAA = cerebral amyloid angiopathy; CMB = cerebral microbleed

Introduction

Sporadic cerebral amyloid angiopathy (CAA) is a common neuropathological finding in the ageing human brain and an important risk factor for cognitive impairment and lobar intracerebral haemorrhage. On autopsy, ~50–80% of brains of patients with dementia have CAA, which is moderate-to-severe in ~30% of the cases (Ellis *et al.*, 1996; Pfeifer *et al.*, 2002). Even in community-dwelling elderly individuals, moderate-to-severe CAA is observed in ~25% of the brains at autopsy (Arvanitakis *et al.*, 2011*a*; Boyle *et al.*, 2015). Histopathologically, CAA is characterized by the accumulation of amyloid-β in the walls of leptomeningeal and cortical small vessels (Thal *et al.*, 2009). Severe CAA is often accompanied by vasculopathic changes (i.e. morphological changes to the small vessels such as microaneurysms and fibrinoid necrosis) (Love *et al.*, 2014), and multiple cortical parenchymal lesions such as microhaemorrhages and microinfarcts (Haglund *et al.*, 2006; Soontornniyomkij *et al.*, 2010; Kövari *et al.*, 2013; Love *et al.*, 2014). It is believed that these widely distributed lesions in the brain parenchyma contribute to cognitive impairment often observed in patients with CAA (Arvanitakis *et al.*, 2011*b*; Greenberg *et al.*, 2014). Hence, they are potentially important targets for prevention and therapeutic strategies, and may serve as surrogate neuroimaging markers in clinical trials (Greenberg *et al.*, 2014). However, it remains largely unknown to what extend we are currently capturing the whole burden of microhaemorrhages and microinfarcts on clinical *in vivo* MRI, which complicates their use in clinical decision-making and therapeutic trials to date.

Currently, cerebral microbleeds (CMBs) are the key neuroimaging manifestations in CAA (Greenberg *et al.*, 2009). A clinical diagnosis of CAA during life relies on the presence of a large intracerebral haemorrhage, or multiple strictly lobar CMBs, visible as small hypointense round or ovoid lesions on T_2*-weighted MRI (Knudsen *et al.*, 2001; Martinez-Ramirez *et al.*, 2015). Although it is widely believed that CMBs represent old microhaemorrhages in the parenchyma, the exact underlying pathology of these MRI-defined lesions remains to a large extent unclear, because few studies have directly and systematically verified them with pathology (Shoamanesh *et al.*, 2011). Moreover, histological observations from such MRI-pathology studies suggest that not only 'frank' haemorrhages, but also morphological changes to the small vessels or haemorrhagic microinfarcts may be visible as CMBs on MRI (Fazekas *et al.*, 1999; Schrag *et al.*, 2010; van Veluw *et al.*, 2016). But as these correlation studies were primarily performed in post-mortem human brain tissue, it remains unclear how these findings translate to CMBs visible on *in vivo* MRI. Throughout this paper we use the term 'CMB' for the MRI-defined lesion, and 'microhaemorrhage' for the pathological manifestation of an old or acute haemorrhage (based on evidence of intact or degraded erythrocyte extravasation) on histology.

Although microinfarcts have extensively been described in autopsy studies (Haglund *et al.*, 2006; Soontornniyomkij *et al.*, 2010; Kövari *et al.*, 2013), they have long been considered 'invisible' on MRI (Smith *et al.*, 2012). It was recently shown that microinfarcts in cortical areas of the brain can be captured *in vivo* as hyperintense lesions on high resolution T_2-weighted images acquired at 7 T MRI (van Veluw *et al.*, 2013, 2015*a*). Moreover, it was shown that a subset of these lesions is also visible at 3 T MRI (van Dalen *et al.*, 2015; van Veluw *et al.*, 2015*b*). However, it remains unclear if microinfarcts can be captured with (1.5 T) MRI scans used in clinical practice.

In this study, we aimed to gain more insight into the pathological basis of MRI-defined CMBs and microinfarcts in the context of CAA and to explore the proportion of the pathological burden that remains undetected. To this end, we performed high and ultra-high resolution *ex vivo* 7 T MRI and histopathological examination in pathology-proven CAA cases with a high lesion burden on their *in vivo* MRI.

Material and methods

Cohort description and study design

The overall study design is summarized in Fig. 1. We searched across datasets of the Massachusetts General Hospital for patients seen during the period 1997–2012, aged >55, who underwent both brain MRI and brain autopsy. At autopsy, one hemisphere was formalin-fixed and

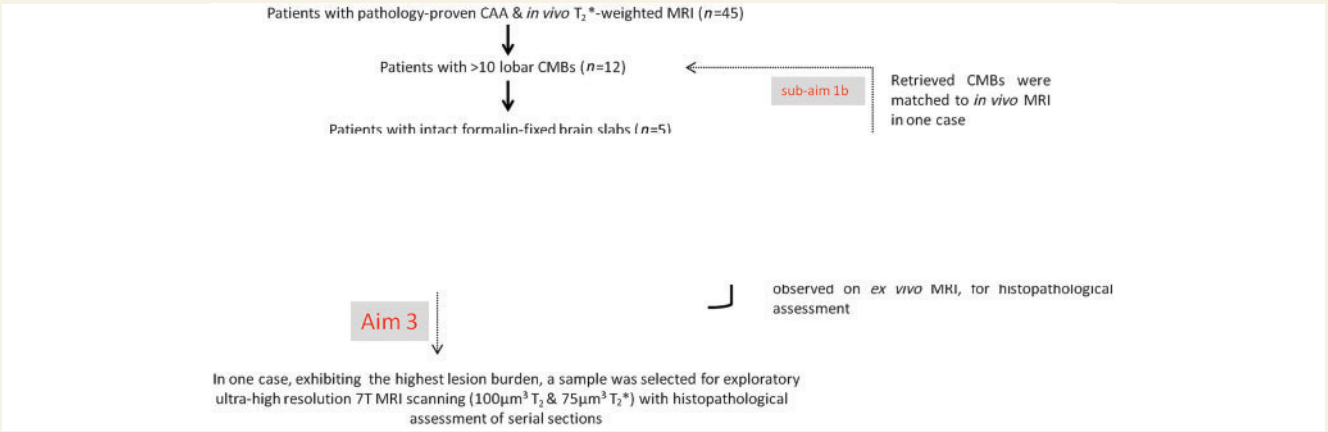

Figure 1 Study design and flowchart. Twelve of 45 patients from the whole cohort had >10 lobar CMBs on their last MRI before death, and were selected for the *ex vivo* MRI study. Upon retrieval of the stored brain slabs from the local neuropathology database, brain tissue proved to be available for 5 of 12 cases. Hence, intact formalin-fixed brain slabs from five cases were selected for *ex vivo* MRI scanning. We first assessed CMBs on the obtained *ex vivo* MRI, followed by detailed histopathological examination of a representative subset of these lesions (Aim 1). In one case with adequate *in vivo* MRI scan quality, we were able to match CMBs observed on *in vivo* MRI to the corresponding *ex vivo* MRI and histopathology sections (sub-Aim 1 b). Second, we assessed microinfarcts on the same *ex vivo* MRI images, followed by detailed histopathological examination of a representative subset of these lesions (Aim 2). Finally, we rescanned one smaller sample cut from a slab containing the highest number of magnetic resonance-observed CMBs, with a dedicated ultra-high resolution *ex vivo* MRI protocol, followed by serial sectioning of the whole tissue. Hence we explored the microvascular abnormalities that are visible at this ultra-high resolution, but remained undetected at high resolution *ex vivo* MRI and *in vivo* MRI, and studied their underlying histopathology (Aim 3).

subjected to routine neuropathological examination. Patients were selected if they showed pathological evidence of mild, moderate or severe CAA on autopsy and had available *in vivo* T_2*-weighted MRI scans (Martinez-Ramirez *et al.*, 2015). Hence, 45 patients met these criteria. Two experienced raters (S.J.v.V and A.L.) assessed CMBs on the last MRI scan before death [inter-rater reliability was excellent; Intraclass Correlation (ICC) = 0.86], followed by a consensus meeting to obtain definite CMB ratings. Next, to ensure a high lesion yield for *ex vivo* MRI and subsequent histological examination, patients with >10 lobar CMBs were selected for inclusion in our study. The local institutional review board approved the study and written informed consent was obtained prior to autopsy.

To verify the pathology of magnetic resonance-observed CMBs (Aim 1), we first assessed CMBs on the obtained *ex vivo* MRI images according to well established rating criteria (Gregoire *et al.*, 2009; Wardlaw *et al.*, 2013), followed by detailed histopathological examination of a representative subset of these lesions. In one case we directly verified CMBs observed on *in vivo* MRI with histopathology (sub-Aim 1b), by registering the *in vivo* MRI to the *ex vivo* MRI and the histology sections. To verify the pathology of magnetic resonance-observed microinfarcts (Aim 2), we next assessed microinfarcts on the same *ex vivo* MRI images according to previously proposed rating criteria (van Veluw *et al.*, 2015*a*, *c*), followed by detailed histopathological examination of a representative subset of these lesions. Finally, we aimed to explore the microvascular abnormalities that are visible at ultra-high resolution MRI, but remained undetected at high resolution *ex vivo* MRI and *in vivo* MRI (Aim 3). Hence, we rescanned one smaller tissue sample, cut from a slab containing the highest number of lesions (based on the high resolution scan), with an ultra-high resolution *ex vivo* MRI protocol, and followed by serial sectioning of the entire sample.

Brain tissue

For each case, four or five formalin-fixed 5–10-mm thick continuous coronal brain slabs were selected from the brain area with the highest burden of CMBs on the last *in vivo* MRI scan prior to death. For each *ex vivo* scan session, slabs submerged in 10% formalin were placed in the correct anatomical order in a glass container that fitted in the head coil of the MRI scanner. Care was taken to avoid air bubbles by gently shaking the tissue.

Ex vivo MRI protocol

Scans were acquired overnight on a whole-body 7 T magnetic resonance Siemens MAGNETOM scanner with a custom built 32-channel head coil. The optimized scan protocol included spoiled gradient echo T_2*-weighted (FLASH) and T_2-weighted acquisitions. FLASH consisted of multiple gradient echoes (multiple echo times) and multiple flip angles, combined using the FLASH steady-state equation (Fischl *et al.*, 2004; Deoni *et al.*, 2005). T_2-weighted volumes were obtained by averaging multiple turbo spin echo (TSE) acquisitions with identical scan parameters. The parameters for the high resolution FLASH acquisitions were as follows: one run each of four flip angles

(10°, 20°, 30° and 40°), matrix 480 × 480, 384 partitions, voxel size 200 × 200 × 200 μm^3, 96 × 96 × 76.8 mm^3 volume, repetition time = 20 ms, single echo echo time = 8.67 ms, bandwidth = 180 Hz/px, scan duration 61 min 26 s, processed to fit proton density, T_1 and T_2* and combined to synthesize the original flip angles from all four scans. The parameters for the high resolution TSE acquisitions were as follows: matrix 330 × 320, 120 partitions, voxel size 300 × 300 × 300 μm^3, 99 × 96 × 36 mm^3 volume, flip angle = 120°, turbo factor 9, repetition time = 1000 ms, echo time = 63 ms, bandwidth = 401 Hz/px, scan duration 60 min 1 s, with four averages.

Ex vivo MRI rating and sampling

One experienced observer (S.J.v.V.) screened the acquired high resolution *ex vivo* MRI scans for CMBs (intra-rater reliability was excellent; ICC = 0.94) and cortical microinfarcts (intra-rater reliability was excellent; ICC = 0.83), blinded to clinical data and *in vivo* MRI. CMBs were defined as focal, round or ovoid hypointense lesions on T_2- and T_2*-weighted magnetic resonance images, <10 mm in greatest dimension (measured on T_2*), according to well-established rating criteria (Gregoire *et al.*, 2009; Wardlaw *et al.*, 2013). Because T_2*-weighted *ex vivo* MRI is highly susceptible to artefacts caused by remaining air bubbles trapped in sulci and between slabs, the T_2-weighted scan was used to discriminate actual CMBs from such air artefacts. Cortical microinfarcts were defined as focal hyperintense lesions on T_2-weighted MRI, isointense on T_2*, <5 mm in greatest dimension, located within the cortical ribbon, according to previously proposed rating criteria (van Veluw *et al.*, 2015*a*, *c*). A second observer (A.C.) screened the same *ex vivo* MRI images to establish inter-rater reliability, which proved to be excellent for CMBs (ICC = 0.80) and good for cortical microinfarcts (ICC = 0.70). Microbleed and microinfarct rating was performed using an in-house developed tool, incorporated in MeVisLab (MeVis Medical Solutions AG, Bremen, Germany).

Next, per case several samples were taken, targeting representative CMBs and microinfarcts for histopathological analysis. These pathological samples measured ~20 × 15 × 5 mm^3 to fit a tissue cassette.

Histopathological analysis

Samples were dehydrated, embedded in paraffin, and cut in 6-μm thick serial sections on a microtome. Lesion retrieval was guided by the corresponding *ex vivo* MRI, based on tissue architecture and estimated depth of the lesion within the tissue blocks. At the estimated lesion location, sections were collected on glass slides for standard haematoxylin and eosin staining. Adjacent sections were collected and saved for immunohistochemistry. Next, haematoxylin and eosin sections were matched with the *ex vivo* MRI scans, to verify retrieval of targeted CMBs and microinfarcts on MRI. If necessary, additional sections were cut at different depths. In case of positive retrieval, adjacent sections were stained for GFAP, amyloid-β, and Perl's iron. All histopathological findings were independently confirmed by an experienced board-certified neuropathologist (M.P.F.), blinded to MRI findings and clinical data. The neuropathologist scored the lesions for presence of erythrocyte extravasation (indicative of a recent haemorrhagic event), blood-breakdown products (such as haematoidin or haemosiderin, indicative of subacute or old haemorrhages), areas of tissue pallor corresponding to microinfarction, and vasculopathies (i.e. morphological changes to the small vessels, such as fibrin in the vessel wall or microaneurysms).

Ex vivo MRI–*in vivo* MRI registration

In one case, matching of the whole *ex vivo* scanned brain volume (consisting of four continuous 10-mm thick brain slabs) to the previously obtained *in vivo* MRI was feasible, based on preservation of the anatomical order of these slabs and availability of a high quality *in vivo* 3D T_1-weighted 1.5 T MRI for reliable registration. The interval between last *in vivo* MRI and death in this case was 1 year and 14 days. Registration was performed using manual and affine registration approaches contained in the Freesurfer toolbox (surfer.nmr.mgh.harvard.edu) (Fischl, 2012) based on landmarks in the relevant cortical ribbon.

Exploratory ultra-high resolution *ex vivo* MRI and histopathology

To explore the pathological burden that remained undetected at high resolution *ex vivo* MRI (and clinical resolution *in vivo* MRI), a small area from one of the slabs containing a high lesion burden was selected and scanned with a dedicated ultra-high resolution protocol. Subsequently the sample was cut into serial sections as a whole for detailed histopathological analysis. For this exploratory study, one area with the highest number of CMBs on the obtained high resolution *ex vivo* MRI was chosen and sampled to fit in a 50 ml falcon tube, submerged in Fomblin® (Solvay Solexis). The tube was placed in a custom built (four-turn) solenoid coil (with an inner diameter of 30 mm), and scanned for ~39 h using the 7 T MRI scanner described above. The parameters for the ultra-high resolution FLASH acquisitions were as follows: four runs each of four flip angles (10°, 20°, 30° and 40°), matrix 448 × 896, 352 partitions, voxel size 75 × 75 × 75 μm^3, 33.6 × 67.2 × 26.4 mm^3 volume, repetition time = 45 ms, single echo echo time = 15.8 ms, bandwidth = 70 Hz/px, scan duration 1 h 58 min 9 s, processed to fit proton density, T_1 and T_2* and combined to synthesize the original flip angles from all 16 scans. The parameters for the ultra-high resolution TSE acquisitions were as follows: matrix 320 × 512, 128 partitions, voxel size 100 × 100 × 100 μm^3, 32 × 51.2 × 12.8 mm^3 volume, flip angle = 120°, turbo factor = 9, repetition

Table 1 Case characteristics and *ex vivo* MRI findings

Case ID	Sex	Lobar CMB number on *in vivo* MRI (field strength)		Age at death (years)	Medical history[a]	Cause of death[a]	MRI–death interval	Slabs subjected to *ex vivo* MRI	Cortical CMBs on *ex vivo* MRI (7 T)	Cortical CMIs on *ex vivo* MRI (7 T)	General pathology findings[b]
		Whole brain	ROI								
1	F	12 (1.5 T)	7	81	Dementia	Aspiration bronchopneumonia	1 y 14 d	4 R frontal	30	0	Mild CAA (VS 2); AD (BB III); LBD (B V); moderate hypertensive CVD
2	F	70 (1.5 T)	18	87	Dementia, left thalamic stroke, CAA, hypertension	Unknown	7 d	5 L occipital	72	17	Moderate CAA (VS 3); AD (BB III); moderate hypertensive CVD
3	M	44 (1.5 T)	11	87	Dementia, CAA with prior intracerebral haemorrhages	Intracerebral haemorrhage	2 y 14 d	5 R occipital[c]	19	27	Severe CAA (VS 4); AD (BB IV); primary intracerebral haemorrhage; moderate hypertensive CVD
4	M	31 (1.5 T)	5	93	Dementia	Unknown	6 y 306 d	5 R frontal	25	4	Severe CAA (VS 4); AD (BB VI); severe hypertensive CVD
5	M	42 (3 T)	25	77	Dementia	Unknown	4 y 302 d	5 R occipital	25	0	Moderate CAA (VS 3); AD (BB VI); mild hypertensive CVD

[a]Extracted from medical records.
[b]Extracted from final pathology report.
[c]Two of five slabs were not assessed for CMBs and microinfarcts, because a large portion of this tissue showed haemorrhagic infarction on *ex vivo* MRI.
AD = Alzheimer's disease pathology; B = Braak; BB = Braak and Braak; CMI = microinfarct; CVD = cerebrovascular disease pathology; ICH = intracerebral haemorrhage; LBD = Lewy body disease pathology; ROI = region of interest; VS = Vonsattel scale.

time = 1500 ms, echo time = 79 ms, bandwidth = 148 Hz/px (dwell 6600 ns), scan duration 1 h 55 min 14 s, with four averages. The obtained ultra-high resolution MRI scans can be found in the Supplementary material.

Next, the sample was cut in half, to fit two standard tissue cassettes. After processing and paraffin embedding, 6-µm thick serial sections were taken from both blocks and stained successively with haematoxylin and eosin and amyloid-β, aiming for every fifth and sixth section. Next, the sections were matched with the obtained ultra-high resolution *ex vivo* MRI scans, and lesions were studied both on MRI and histopathology.

Results

Histopathology of *ex vivo* magnetic resonance-observed cerebral microbleeds

Aim 1

Brain slabs from five cases (mean age 85 ± 6 years) were selected for *ex vivo* MRI scanning (Fig. 1). Case characteristics and *ex vivo* MRI findings are presented in Table 1. Other *in vivo* MRI findings can be found in Supplementary Table 1. In total, 171 CMBs were observed on *ex vivo* MRI of the examined slabs, compared to ~66 CMBs in the same areas on the corresponding *in vivo* clinical MRI scans of these cases. Interestingly, in one case that underwent 3 T susceptibility-weighted MRI, the same number of CMBs was observed both *ex vivo* as well as *in vivo* (Table 1). All CMBs observed on *ex vivo* MRI were located in the cortical ribbon, no CMBs were observed in the white matter. In total, 20 CMBs—observed on *ex vivo* MRI—were sampled for histopathological examination. Thirteen of 20 CMBs could be retrieved on the corresponding haematoxylin and eosin sections, whereas seven were missed because of MRI-histopathology mismatching. Eight represented old or subacute microhaemorrhages characterized by (iron positive) focal haemosiderin deposits with or without haematoidin (Fig. 2). They appeared more than four-times larger on high-resolution T_2*-weighted MRI (mean size 1.4 ± 0.6 mm) compared to their actual size on the haematoxylin and eosin section (mean size 0.3 ± 0.2 mm; paired samples *t*-test 7.5, $P < 0.001$). Five represented acute microhaemorrhages characterized by a focal accumulation of intact erythrocytes (Fig. 2). One acute microhaemorrhage was negative for iron staining, three were accompanied by only a few iron-positive haemosiderin deposits, and one demonstrated many iron-positive haemosiderin deposits suggesting that the involved vessel had ruptured before. The size of these acute microhaemorrhages on T_2*-weighted MRI (mean size 1.3 ± 0.6 mm) was similar to their actual size on the haematoxylin and eosin section (mean size 0.9 ± 0.6 mm; paired samples *t*-test 2.8, $P = 0.048$).

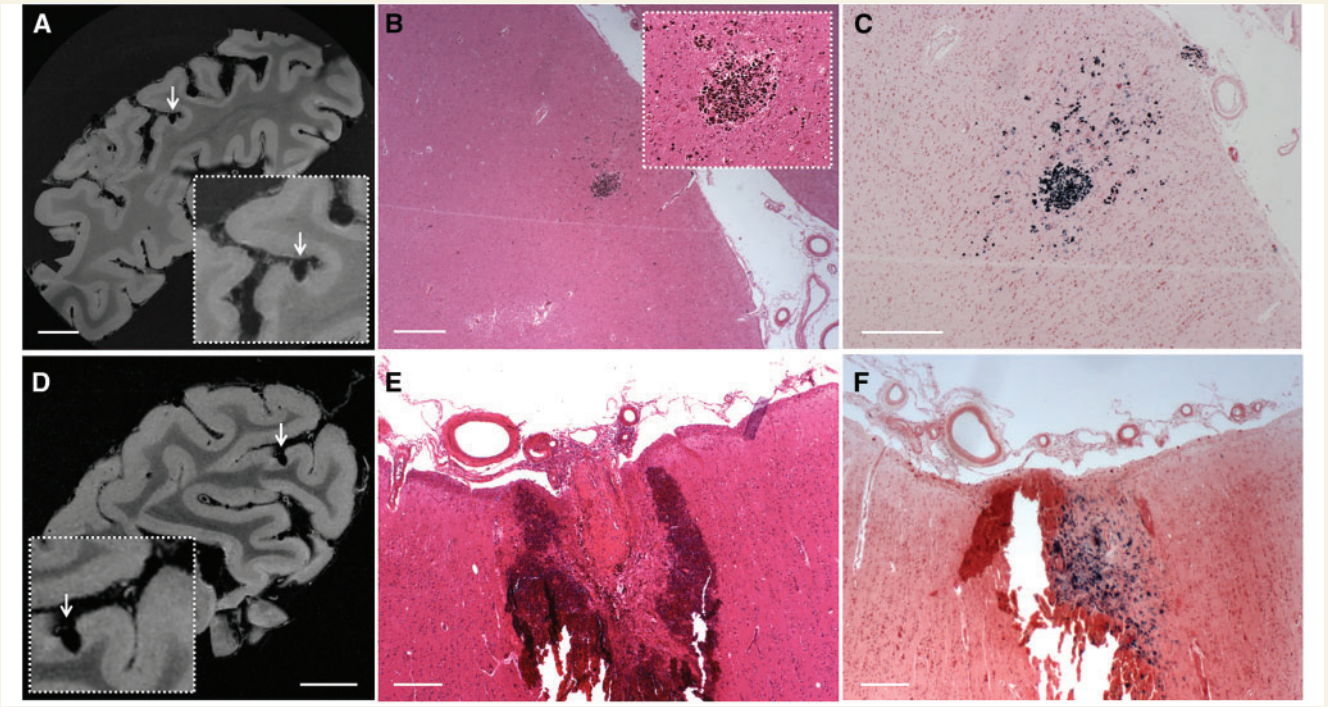

Figure 2 Histopathology of representative examples of magnetic resonance-observed microbleeds. (**A–C**) A cortical microbleed observed on *ex vivo* T_2*-weighted MRI in Case 5 (**A**; arrow) was sampled for histopathological analysis and matched with a focal accumulation of haemosiderin-containing macrophages on haematoxylin and eosin, representing an old microhaemorrhage (**B**). The adjacent section was positive for iron (**C**). Scale bar in **A** = 4 mm; **B** and **C** = 500 μm. (**D–F**) A cortical microbleed observed on *ex vivo* T_2*-weighted MRI in Case 2 (**D**; arrow) was sampled for histopathological analysis and matched with a focal accumulation of erythrocytes close to a ruptured vessel, representing an acute microhaemorrhage (**E**). The adjacent section was partly positive for iron, suggesting that the same vessel had ruptured before (**F**). Scale bar in **D** = 4 mm; **E** and **F** = 250 μm.

Histopathology of *in vivo* magnetic resonance-observed cerebral microbleeds

We were able to register the *ex vivo* 7 T MRI to the previously acquired *in vivo* 1.5 T MRI in Case 1, allowing a direct validation of *in vivo* observed CMBs. In this volume, 30 CMBs were visible on *ex vivo* MRI, compared to seven on the corresponding *in vivo* T_2*-weighted MRI. All seven *in vivo* observed CMBs could be matched with CMBs on *ex vivo* MRI (Fig. 3). Three *in vivo* observed CMBs were sampled as part of Aim 1 (see above), and proved to be old microhaemorrhages on microscopy. Of note, these three old microhaemorrhages measured <300 μm on the haematoxylin and eosin section. No microinfarcts were observed in this case, or on *ex vivo* MRI, or on *in vivo* MRI.

Histopathology of *ex vivo* magnetic resonance-observed microinfarcts

Aim 2

A total number of 48 cortical microinfarcts were present on *ex vivo* MRI of the examined slabs of three of the five cases. In two cases we did not observe any microinfarcts on *ex vivo* MRI. None of the cortical microinfarcts were retrospectively visible on the corresponding clinical low resolution *in vivo* fluid-attenuated inversion recovery (FLAIR) or T_1-weighted MRI scans of these cases. In terms of their spatial distribution, CMBs and microinfarcts did not co-localize on *ex vivo* MRI. Microinfarcts, but not CMBs, tended to cluster. In total 10 cortical microinfarcts—observed on *ex vivo* MRI—were sampled for histopathological examination. Nine of 10 microinfarcts could be retrieved on the corresponding haematoxylin and eosin sections. Four represented chronic microinfarcts characterized by pallor, tissue loss, and gliosis (confirmed by GFAP staining) (Fig. 4). Five represented acute microinfarcts characterized by tissue pallor, and ischaemic or shrunken neurons (Fig. 4). None of the microinfarcts were positive for iron. The size of the microinfarcts on T_2-weighted MRI (mean size 1.5 ± 1.0 mm) was similar to their actual size on the haematoxylin and eosin section (mean size 1.0 ± 0.8 mm; paired samples *t*-test 1.4, $P = 0.218$). It should be noted that four of five acute microinfarcts were observed in a case that also had a larger cortical intracerebral haemorrhage in non-adjacent areas. Hence, it cannot be excluded that these microinfarcts were related to the larger event.

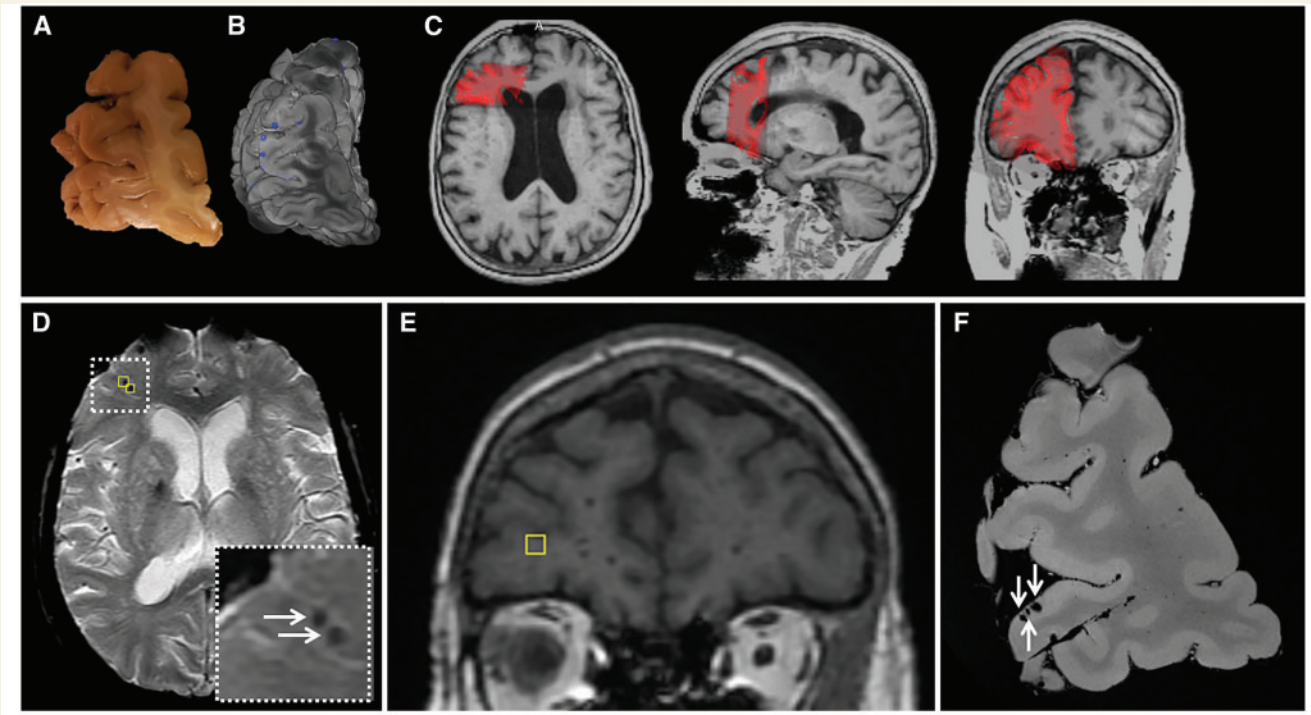

Figure 3 Matched microbleeds between *in vivo* and *ex vivo* MRI, after registration. From one case the tissue volume that was subjected to *ex vivo* MRI (**A** and **B**) could be matched with the corresponding *in vivo* MRI, acquired 1 year and 14 days ante-mortem (**C**). First, the *ex vivo* T_2*-weighted MRI (**B**) was matched to the *in vivo* 3D T_1-weighted 1.5 T MRI, by means of manual and linear registration (**C**). **B** represents a volume rendering of the four continuous slabs taken from the right frontal area stacked on top of each other. The blue dots represent microbleeds observed on *ex vivo* MRI. Second, observed microbleeds on the *in vivo* T_2*-weighted 1.5 T MRI (**D**) were registered to the coronal *in vivo* T_1-weighted MRI image (**E**; marker corresponds to left marker in **D**) and compared to the volume-matched *ex vivo* T_2*-weighted MRI image (**F**). Hence, all seven microbleeds that were found on *in vivo* MRI in this case could be matched to microbleeds on the corresponding *ex vivo* MRI. Three microbleeds, which were both identified on *in vivo* (**D**, two are captured in this transversal view) and *ex vivo* MRI (**F**, all three are captured in this coronal view), were subsequently sampled for histopathological examination and proved to be old microhaemorrhages on microscopy.

Exploratory ultra-high resolution *ex vivo* MRI

Aim 3

To explore the pathological burden that remained undetected at high resolution *ex vivo* MRI (and clinical resolution *in vivo* MRI), we subjected a smaller sample from Case 2 (which was subsequently cut into serial sections) to an ultra-high resolution scan protocol. This chosen region of interest contained 24 CMBs as detected on high resolution (200 μm^3 T_2*-weighted) *ex vivo* MRI. Four CMBs were located at the borders of the processed tissue blocks and could therefore not reliably be assessed on histology, leaving 20 CMBs for histopathological examination. Due to serial sectioning all 20 CMBs were retrieved on histology. Eighteen of 20 CMBs were classified as either acute or old microhaemorrhages upon examination of the histopathologic sections, whereas two CMBs corresponded to vasculopathies (i.e. morphological changes to the vessels without parenchymal damage). This resulted in a positive predictive value of 90% (95% CI 0.68–0.99) for CMBs detected at 200 μm^3 T_2*-weighted 7 T MRI.

On the ultra-high resolution (75 μm^3 T_2*-weighted) *ex vivo* MRI an additional 48 smaller hypointense cortical lesions were identified in the same volume, which were not identified as CMBs on the corresponding high resolution *ex vivo* MRI. Eleven of them had a round or ovoid shape, and hence were considered 'typical' (although very small) CMBs, whereas 31 had a more vessel-like and six an irregular appearance, hence considered 'atypical' CMBs. Twenty-seven of the 48 additional hypointense lesions could reliably be identified on histopathology, of which 20 (74.1%) corresponded to vasculopathies (Fig. 5), one to a haemorrhagic microinfarct, and only six (22.2%) to actual haemorrhages. On histopathology, such vasculopathies were not found in CMB-negative areas.

We also evaluated the sensitivity of high versus ultra-high resolution *ex vivo* MRI for microinfarct detection. The same volume contained two cortical microinfarcts as detected on high resolution (300 μm^3 T_2-weighted) *ex vivo* MRI, which were both histologically confirmed. On the ultra-high resolution (100 μm^3 T_2-weighted) *ex vivo* MRI, no additional microinfarcts were observed. After screening all obtained serial histological sections from this particular sample, however, nine microinfarcts were found on

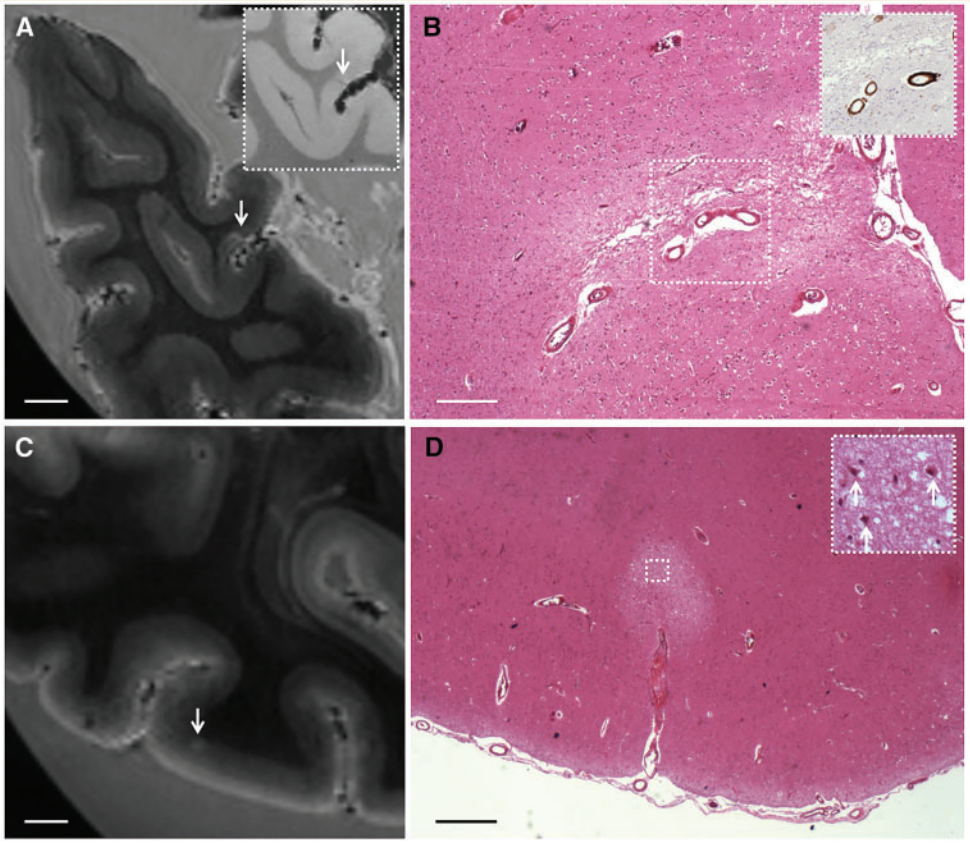

Figure 4 Histopathology of representative examples of magnetic resonance-observed microinfarcts. (**A** and **B**) A cortical microinfarct observed on *ex vivo* T_2-weighted MRI in Case 3 (**A**; arrow; inset is T_2*-weighted MRI) was sampled for histopathological analysis and matched with a region of pallor, tissue loss, and gliosis on haematoxylin and eosin, representing a chronic microinfarct (**B**). The inset in **B** shows amyloid-β positive cortical vessels associated with the microinfarct, observed on an adjacent section stained for amyloid-β. Scale bars in **A** = 4 mm; **B** = 250 μm. (**C** and **D**) A cortical microinfarct observed on *ex vivo* T_2-weighted MRI in Case 2 (**C**; arrow) was sampled for histopathological analysis and matched with a region of tissue pallor containing ischaemic neurons (arrows; inset), representing an acute microinfarct (**D**). Scale bars in **C** = 4 mm; **D** = 500 μm.

microscopic examination. Six were in retrospect visible at the ultra-high resolution T_2-weighted MRI scan only (Fig. 5), whereas three were too small to be visible on MRI (mean size on haematoxylin and eosin sections 0.2 ± 0.1 mm). Noteworthy, four microinfarcts on pathology were accompanied by several haemosiderin deposits, and hence interpreted as haemorrhagic microinfarcts. Their appearance on MRI was either hypointense or inhomogeneous (partly hypointense/hyperintense).

Discussion

This study aimed to gain more insight in the pathological basis of MRI-defined CMBs and microinfarcts, in the context of CAA and to explore the pathological burden that remains undetected. Our combined *in vivo–ex vivo*–histopathology approach resulted in several key new insights: (i) lobar CMBs on clinical *in vivo* MRI in patients with CAA are specific for haemorrhagic pathology; (ii) although high resolution (200 μm isotropic resolution) *ex vivo* MRI was able to detect additional CMBs beyond regular clinical resolution *in vivo* MRI, further increased spatial resolution (up to 75 μm isotropic) resulted in the detection of more 'non-haemorrhagic' CAA pathology (i.e. vasculopathies). These vasculopathies appeared as CMBs on *ex vivo* MRI and hence reduced specificity for the detection of 'frank' haemorrhages at this resolution; and (iii) in contrast to CMBs, the vast majority of microinfarcts currently remain under the detection limits of clinical *in vivo* MRI and even high resolution *ex vivo* MRI. Hence, the sensitivity for microinfarct detection does benefit substantially from an increased spatial resolution.

Our findings suggest that cortical CMBs on MRI in patients with pathology-proven CAA correspond well to 'frank' haemorrhages. All 13 retrieved CMBs (Aim 1) proved to be either acute or old microhaemorrhages (based on evidence of extravasations of intact or degraded erythrocytes on histopathology). Seven CMBs could not be retrieved on histology, most likely due to mismatching between the MRI scans and the histology sections. It cannot be excluded, however, that these missed lesions may have

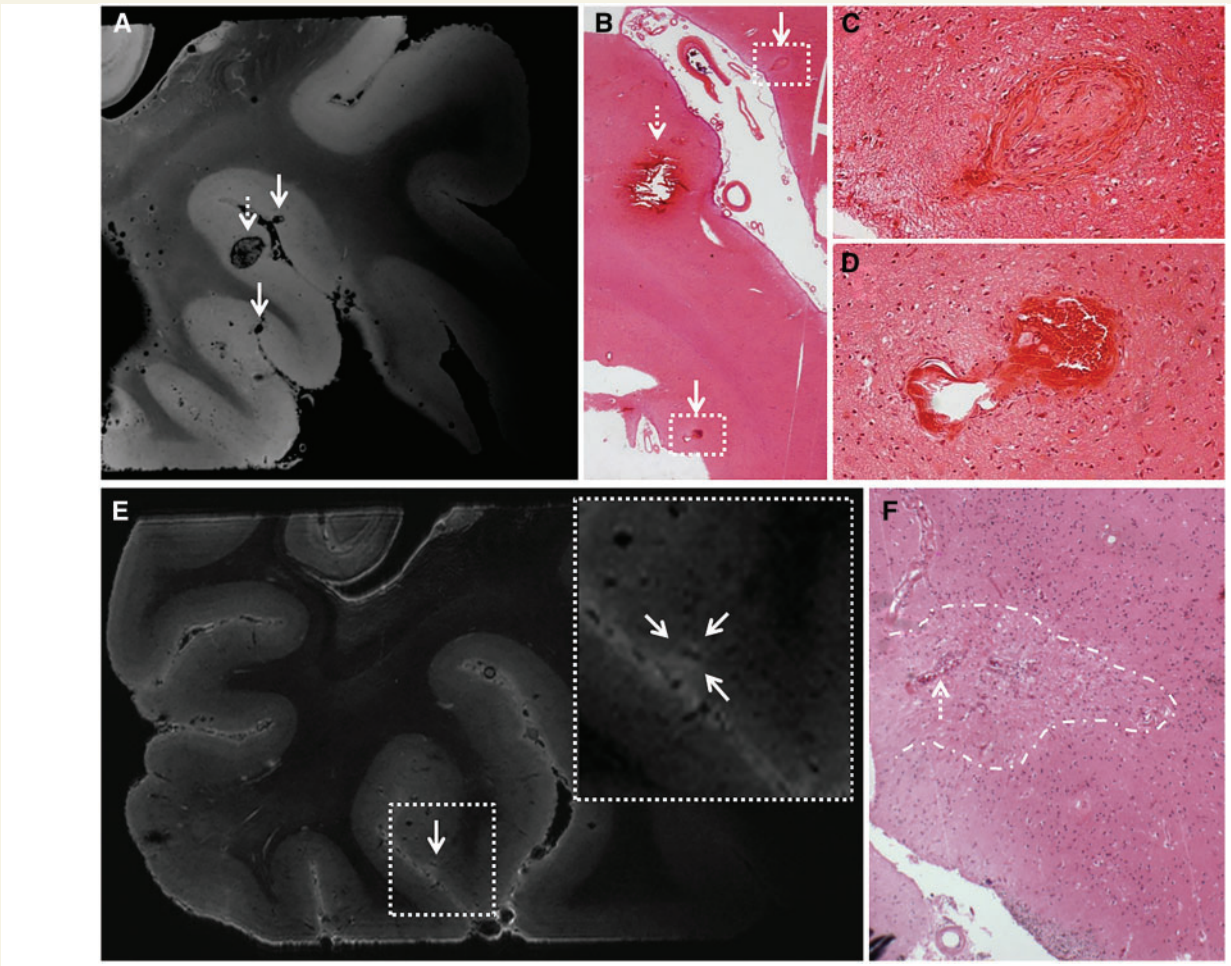

Figure 5 Exploratory ultra-high resolution *ex vivo* MRI. Ultra-high resolution *ex vivo* magnetic resonance images of a sampled brain area from Case 2 reveal striking detail of CAA-related pathology. *Top row*: Here we show three representative microbleeds that were identified on the ultra-high resolution T_2*-weighted *ex vivo* magnetic resonance image (voxel size 75 μm^3), of which the larger one (broken arrow) was also visible at the corresponding high resolution T_2*-weighted *ex vivo* magnetic resonance image (voxel size 200 μm^3) (**A**). This microbleed corresponded to a recent microhaemorrhage on haematoxylin and eosin, characterized by a focal accumulation of intact erythrocytes (broken arrow; **B**). The hypointense lesions (arrows) that were not rated as microbleeds at high-resolution T_2*-weighted *ex vivo* MRI, proved to be vasculopathies on haematoxylin and eosin, without parenchymal tissue injury (arrows; **B**, enlarged in **C** and **D**). The vasculopathy in **C** resembles an occluded vessel containing fibrin deposits. The vasculopathy in **D** resembles a microaneurysm. *Bottom row*: Here we show a microinfarct that was identified on microscopic examination of the serial histological sections taken from this sample (**F**), and retrospectively could be identified as a hyperintense lesion on the corresponding ultra-high resolution T_2-weighted *ex vivo* magnetic resonance image (voxel size 100 μm^3) (**E**), whereas it escaped detection at high-resolution T_2-weighted *ex vivo* MRI (voxel size 300 μm^3). Note the vessel at the centre of this microinfarct (broken arrow in **F**), which can be distinguished on the scan (hypointense structure within the hyperintense lesion in **E**).

represented other types of pathology or abnormalities related to post-mortem imaging (e.g. post-mortem thrombi in penetrating vessels or trapped air bubbles). Importantly, the fact that serial sectioning (in the context of Aim 3) did reveal all targeted CMBs ($n = 20$) on histology, supports the interpretation that the seven missing CMBs in the analysis of Aim 1 were indeed caused by mismatching problems and did not in fact represent false-positive CMBs. Being able to compare these additional 20 CMBs to the histopathology-based standard (provided by the serial sections) resulted in a positive predictive value of 90% (only two CMBs did not represent frank haemorrhages, but vasculopathies). This underlines the high specificity of CMBs to represent actual haemorrhagic pathology. Interestingly, by lining up the *ex vivo* MRI with *in vivo* MRI in one case, we found that even very small (< 300 µm) old microhaemorrhages on pathology can still be detected on *in vivo* MRI. Furthermore, the observation that old—iron-positive—microhaemorrhages bloom more than acute—iron-negative—microhaemorrhages is in line with previous observations (Schrag *et al.*, 2010; van Veluw *et al.*, 2016). It has also been suggested that smaller microhaemorrhages bloom more than larger (Schrag *et al.*, 2010), which may also explain our current and previous

observations, as old microhaemorrhages were generally smaller on histology than the acute ones. Previous studies have demonstrated that it is possible to quantify iron content of individual lesions on MRI (Klohs *et al.*, 2011). This may be an interesting avenue to help discriminate old from acute microhaemorrhages *in vivo*. Moreover, we noticed that acute haemorrhages sometimes generate heterogeneous signal intensities on MRI when they consist of partly intact and partly lysed erythrocytes (Fig. 5; van Veluw *et al.*, 2016). This could also potentially—when not limited by spatial resolution—help discriminate acute from old bleeding events *in vivo*.

In this study, on average 2.5-times more CMBs were identified on high-resolution *ex vivo* 7 T MRI compared to clinical *in vivo* MRI. Interestingly, such an enhanced detection was not observed for the one individual who underwent 3 T susceptibility-weighted MRI *in vivo*. This suggests, and confirms previous observations (Nandigam *et al.*, 2009), that 3 T MRI is more sensitive for CMB detection compared to lower resolution 1.5 T MRI. It cannot be excluded that a number of CMBs may have occurred in the interval between last MRI and death. However, this seems unlikely because in one patient (Case 2; Table 1) who had her last MRI 7 days before she died, *ex vivo* MRI detected four-times more CMBs than *in vivo* MRI. Considering it unlikely that the extra CMBs occurred within those 7 days, it underlines the higher sensitivity of *ex vivo* 7 T MRI for the detection of CMBs compared to clinical *in vivo* MRI. This is in line with previous studies, demonstrating that 7 T *in vivo* MRI results in increased detection of CMBs compared to 1.5 T MRI (Conijn *et al.*, 2011; Ni *et al.*, 2015) and 3 T MRI (Brundel *et al.*, 2012). This higher sensitivity seems to be mainly driven by the higher spatial resolution of 7 T MRI and different image contrast, compared to conventional MRI (Brundel *et al.*, 2012; van Veluw *et al.*, 2014). Markedly, all *ex vivo* magnetic resonance-observed CMBs in this study were located in the cortical ribbon, which is consistent with a previous high-resolution *ex vivo* (van Veluw *et al.*, 2016) and *in vivo* 7 T MRI study (Ni *et al.*, 2015).

We found that further increasing the spatial resolution to 75 μm^3 using ultra-high resolution *ex vivo* MRI results in the detection of other CAA-related non-haemorrhagic pathologies. This is in line with previous *ex vivo* MRI-histopathology correlation studies in the context of CAA, which suggested that not all CMBs represent actual haemorrhages, but that some of them may represent non-haemorrhagic vasculopathies (Schrag *et al.*, 2010; Fisher, 2014; van Veluw *et al.*, 2016). In one of our recent *ex vivo* 7 T MRI-histopathology studies in cases with severe CAA, we found that 4 of 17 cortical CMBs represented vasculopathies instead of haemorrhages (van Veluw *et al.*, 2016). Vasculopathies are frequently observed in the context of more severe CAA, and may represent the vessels that are most likely to bleed upon disease progression (Vonsattel *et al.*, 1991; Love *et al.*, 2014). Hence, these vessels are interesting targets to get to the mechanisms underlying haemorrhage formation in CAA. Ultra-high resolution MRI provides a unique tool to accurately target these lesions for further detailed histopathological analysis, and should be used in future studies. For example, determining absence or presence of vascular amyloid-β in such vessels would provide invaluable insight into the role of vascular amyloid-β in haemorrhage formation.

In contrast to CMBs, clinical *in vivo* MRI highly underestimates the detection of cortical microinfarcts, as none of the microinfarcts observed on *ex vivo* MRI proved to be visible on *in vivo* 1.5 T MRI. Previous studies have shown, however, that increasing spatial resolution, either by means of *in vivo* 7 T MRI (van Veluw *et al.*, 2013; van Rooden *et al.*, 2014; Dieleman *et al.*, 2016) or *ex vivo* MRI (van Veluw *et al.*, 2015*a*), strongly increases sensitivity for microinfarct detection. Our findings showed that cortical microinfarcts have a similar size on *ex vivo* MRI compared to their size on histology. The improved sensitivity of high resolution *ex vivo* or *in vivo* MRI for microinfarct detection (as compared to clinical *in vivo* MRI) seems largely driven by a higher spatial resolution. In our previous work, we suggested to use T_1-weighted MRI for the detection of microinfarcts on clinical 3 T MRI scans (van Veluw *et al.*, 2015*b*, *c*), as these images both exhibit high spatial resolution and great contrast between grey and white matter (unlike most clinically-used FLAIR scans). The clinical *in vivo* 1.5 T MRI protocol that most subjects in this study underwent included a poor quality T_1-weighted sequence, which explains why no microinfarcts could retrospectively be observed on *in vivo* MRI here. One patient who underwent 3 T MRI *in vivo* did not show any microinfarcts *ex vivo*. Hence, we could unfortunately not verify enhanced detection of microinfarcts at 3 T (as opposed to 1.5 T) in this case.

This is one of the first studies investigating the co-occurrence of CMBs and microinfarcts on MRI in the context of CAA. We found no topographical co-localization of CMBs and microinfarcts. Moreover, microinfarcts were only found in the cases with more severe CAA, which is consistent with previous studies (Haglund *et al.*, 2006; Soontornniyomkij *et al.*, 2010; Kövari *et al.*, 2013). This suggests that microinfarcts are an expression of more severe CAA burden, and may also point to different mechanisms underlying microhaemorrhage and microinfarct formation. Although microhaemorrhages are considered to be the result of severe CAA as well (Vonsattel *et al.*, 1991; Love *et al.*, 2014), the positive association between multiple CMBs on MRI and more severe CAA on pathology has not convincingly been demonstrated yet (Charidimou *et al.*, 2016). Likewise, although all our cases had >10 CMBs on *in vivo* MRI, only two cases proved to have the highest CAA severity score (according to the Vonsattel criteria) on neuropathological examination (Table 1). This raises intriguing questions about the direct link between CAA severity and microhaemorrhage formation at the single vessel level, a topic for future studies. The observation of haemorrhagic microinfarcts in this study

and in previous studies is of interest as it suggests different mechanisms (both erythrocyte extravasation and infarction) associated with the same vessel.

The strength of this study is that we combined *in vivo* MRI with *ex vivo* MRI and in-depth histopathology. A clear limitation was the availability of only a small number of cases. However, using high quality 7 T MRI scan protocols we were able to assess both high numbers of CMBs and microinfarcts on MRI in the context of CAA, investigate their underlying pathology, and to translate our findings to clinical *in vivo* MRI. It should be noted that the implications derived from these findings solely relate to cortical microvascular lesions. As the slabs subjected to *ex vivo* MRI in this study did not contain subcortical areas (e.g. basal ganglia), other studies are needed to further investigate the pathology of CMBs in deep areas of the brain, as it has been suggested that they are less specific for haemorrhagic pathology, and they may also be the result of calcifications or ischaemic tissue injury (Janaway *et al.*, 2014). Also, because we purposefully included cases with >10 CMBs (to ensure a high lesion yield on *ex vivo* MRI and histopathology), this may have led to an underestimation of the lesion burden that goes undetected on MRI. Future studies should look at lesion burden on pathology in cases with no visible CMBs on *in vivo* MRI. Furthermore, it remains to be seen how our findings translate to different study samples and disease settings (e.g. hypertension, large intracerebral haemorrhages). Finally, unfortunately most patients underwent relatively low quality *in vivo* 1.5 T MRI, which is not uncommon in clinical practice. Hence, registration of *ex vivo* MRI to *in vivo* was only possible in one case. It would be of interest to replicate this in larger numbers of cases, but the availability of datasets including both high quality *in vivo* MRI scans and subsequent brain autopsy to date is very limited.

Conclusions

The findings of this qualitative *in vivo*–*ex vivo*–histopathology study suggest that current *in vivo* CMB detection in patients with CAA is rather specific for haemorrhages and that increasing resolution to ultra-high levels ($\leqslant 75\,\mu m^3$) results in a drop of specificity due to the detection of more non-haemorrhagic pathology. With respect to microinfarcts, the majority currently escapes detection on clinical *in vivo* and *ex vivo* MRI. Increasing MRI field strength and spatial resolution improves the detection of microinfarcts. Ultra-high resolution *ex vivo* MRI appeared to be a powerful tool to study microvascular pathology in CAA at a detailed level, which may aid in unravelling exact mechanisms leading to haemorrhagic and ischaemic tissue injury in this disease. Finally, CMBs and microinfarcts appear to be the most numerous markers of focal haemorrhage and focal ischaemic injury in small vessel diseases (in particular CAA), and therefore are important candidate biomarkers for clinical trials. Our data show that while we are approaching sensitive and specific methods for imaging CMBs *in vivo*, we are not yet for microinfarcts.

Acknowledgements

The authors would like to thank Thijs van Harten for his help with *ex vivo* to *in vivo* MRI registration.

Funding

This work was supported by an Alzheimer Nederland fellowship [WE 15-2013-07] and a Van Leersum grant of the Royal Dutch Academy of Sciences [2467-VLB-519] to S.J.v.V., an NIH grant [R21AG046657] to A.J.v.d.K., a VIDI grant from ZonMw, The Netherlands Organization for Health Research and Development [91711384] to G.J.B., NIH grants [R01AG047975], [P50AG005134], and [K23AG028726] to A.V., and an NIH grant [R01AG26484] to A.V. and S.M.G.

Supplementary material

Supplementary material is available at *Brain* online.

References

Arvanitakis Z, Leurgans SE, Wang Z, Wilson RS, Bennett DA, Schneider JA. Cerebral amyloid angiopathy pathology and cognitive domains in older persons. Ann Neurol 2011a; 69: 320–7.

Arvanitakis Z, Leurgans SE, Barnes LL, Bennett DA, Schneider JA. Microinfarct pathology, dementia, and cognitive systems. Stroke 2011b; 42: 722–7.

Boyle PA, Yu L, Nag S, Leurgans S, Wilson RS, Bennett DA, et al. Cerebral amyloid angiopathy and cognitive outcomes in community-based older persons. Ann Neurol 2015; 85: 1930–6.

Brundel M, Heringa SM, de Bresser J, Koek HL, Zwanenburg JJ, Kappelle JL, et al. High prevalence of cerebral microbleeds at 7Tesla MRI in patients with early Alzheimer's disease. J Alzheimers Dis 2012; 31: 259–63.

Charidimou AC, Martinez-Ramirez S, Reijmer YD, Oliveira-Filho J, Lauer A, Roongpiboonsopit D, et al. Total MRI small vessel disease burden in cerebral amyloid angiopathy: a concept validation imaging-pathological study. JAMA Neurol 2016; 73: 994–1001.

Conijn MM, Geerlings MI, Biessels GJ, Takahara T, Witkamp TD, Zwanenburg JJ, et al. Cerebral microbleeds on MR imaging: comparison between 1.5 and 7T. AJNR Am J Neuroradiol 2011; 32: 1043–9.

Deoni SC, Peters TM, Rutt BK. High-resolution T1 and T2 mapping of the brain in a clinically acceptable time with DESPOT1 and DESPOT2. Magn Reson Med 2005; 53: 237–41.

Dieleman N, van der Kolk AG, Zwanenburg JJ, Brundel M, Harteveld AA, Biessels GJ, et al. Relations between location and type of intracranial atherosclerosis and parenchymal damage. J Cereb Blood Flow Metab 2016; 36: 1271–80.

Ellis RJ, Olichney JM, Thal LJ, Mirra SS, Morris JC, Beekly D, et al. Cerebral amyloid angiopathy in the brains of patients with Alzheimer's disease: the CERAD experience, Part XV. Neurology 1996; 46: 1592–6.

Fazekas F, Kleinert R, Roob G, Kleinert G, Kapeller P, Schmidt R, et al. Histopathologic analysis of foci of signal loss on gradient-echo T2*-weighted MR images in patients with spontaneous intracerebral hemorrhage: evidence of microangiopathy-related microbleeds. AJNR Am J Neuroradiol 1999; 20: 637–42.

Fischl B. Freesurfer. Neuroimage 2012; 62: 774–81.

Fischl B, Salat DH, van der Kouwe AJ, Makris N, Segonne F, Quinn BT, et al. Sequence-independent segmentation of magnetic resonance images. Neuroimage 2004; 23 (Suppl 1): S69–84.

Fisher M. Cerebral microbleeds: where are we now? Neurology 2014; 83: 1304–5.

Greenberg SM, Al-Shahi Salman R, Biessels GJ, van Buchem M, Cordonnier C, Lee JM, et al. Outcome markers for clinical trials in cerebral amyloid angiopathy. Lancet Neurol 2014; 13: 419–28.

Greenberg SM, Vernooij MW, Cordonnier C, Viswanathan A, Al-Shahi Salman R, Warach S, et al. Cerebral microbleeds: a guide to detection and interpretation. Lancet Neurol 2009; 8: 165–74.

Gregoire SM, Chaudhary UJ, Brown MM, Yousry TA, Kallis C, Jäger HR, et al. The Microbleed Anatomical Rating Scale (MARS): reliability of a tool to map brain microbleeds. Neurology 2009; 73: 1759–66.

Haglund M, Passant U, Sjobeck M, Ghebremedhin E, Englund E. Cerebral amyloid angiopathy and cortical microinfarcts as putative substrates of vascular dementia. Int J Geriatr Psychiatry 2006; 21: 681–7.

Janaway BM, Simpson JE, Hoggard N, Highley JR, Forster G, Drew D, et al. Brain haemosiderin in older people: pathological evidence for an ischaemic origin of magnetic resonance imaging (MRI) microbleeds. Neuropathol Appl Neurobiol 2014; 40: 258–69.

Klohs J, Deistung A, Schweser F, Grandjean J, Dominietto M, Waschkies C, et al. Detection of cerebral microbleeds with quantitative susceptibility mapping in the ArcAbeta mouse model of cerebral amyloidosis. J Cereb Blood Flow Metab 2011; 31: 2282–92.

Knudsen KA, Rosand J, Karluk D, Greenberg SM. Clinical diagnosis of cerebral amyloid angiopathy: validation of the Boston criteria. Neurology 2001; 56: 537–39.

Kövari E, Herrmann FR, Hof PR, Bouras C. The relationship between cerebral amyloid angiopathy and cortical microinfarcts in brain ageing and Alzheimer's disease. Neuropathol Appl Neurobiol 2013; 39: 498–509.

Love S, Chalmers K, Ince P, Esiri M, Attems J, Jellinger K, et al. Development, appraisal, validation and implementation of a consensus protocol for the assessment of cerebral amyloid angiopathy in post-mortem brain tissue. Am J Neurodegener Dis 2014; 3: 19–32.

Martinez-Ramirez S, Romero JR, Shoamanesh A, McKee AC, Van Etten E, Pontes-Neto O, et al. Diagnostic value of lobar microbleeds in individuals without intracerebral hemorrhage. Alzheimers Dement 2015; 11: 1480–8.

Nandigam RNK, Viswanathan A, Delgado P, Skehan ME, Smith EE, Rosand J, et al. MR imaging detection of cerebral microbleeds: effect of susceptibility-weighted imaging, section thickness, and field strength. AJNR Am J Neuroradiol 2009; 30: 338–43.

Ni J, Auriel E, Martinez-Ramirez S, Keil B, Reed AK, Fotiadis P, et al. Cortical localization of microbleeds in cerebral amyloid angiopathy: an ultra high-field 7T MRI study. J Alzheimers Dis 2015; 43: 1325–30.

Pfeifer LA, White LR, Ross GW, Petrovitch H, Launer LJ. Cerebral amyloid angiopathy and cognitive function: the HAAS autopsy study. Neurology 2002; 58: 1629–34.

Schrag M, McAuley G, Pomakian J, Jiffry A, Tung S, Mueller C, et al. Correlation of hypointensities in susceptibility-weighted images to tissue histology in dementia patients with cerebral amyloid angiopathy: a postmortem MRI study. Acta Neuropathol 2010; 119: 291–302.

Shoamanesh A, Kwok CS, Benavente O. Cerebral microbleeds: histopathological correlation of neuroimaging. Cerebrovasc Dis 2011; 32: 528–34.

Smith EE, Schneider JA, Wardlaw JM, Greenberg SM. Cerebral microinfarcts: the invisible lesions. Lancet Neurol 2012; 11: 272–82.

Soontornniyomkij V, Lynch MD, Mermash S, Pomakian J, Badkoobehi H, Clare R, et al. Cerebral microinfarcts associated with severe cerebral beta-amyloid angiopathy. Brain Pathol 2010; 20: 459–67.

Thal DR, Capetillo-Zarate E, Larionov S, Staufenbiel M, Zurbruegg S, Beckmann N. Capillary cerebral amyloid angiopathy is associated with vessel occlusion and cerebral blood flow disturbances. Neurobiol Aging 2009; 30: 1936–48.

van Dalen JW, Scuric EE, van Veluw SJ, Caan MW, Nederveen AJ, Biessels GJ, et al. Cortical microinfarcts detected in vivo on 3 tesla MRI: clinical and radiological correlates. Stroke 2015; 46: 255–7.

van Rooden S, Goos JD, van Opstal AM, Versluis MJ, Webb AG, Blauw GJ, et al. Increased number of microinfarcts in Alzheimer disease at 7-T MR imaging. Radiology 2014; 270: 205–11.

van Veluw SJ, Zwanenburg JJ, Engelen-Lee J, Spliet WG, Hendrikse J, Luijten PR, et al. In vivo detection of cerebral cortical microinfarcts with high-resolution 7T MRI. J Cereb Blood Flow Metab 2013: 33: 322–9.

van Veluw SJ, Zwanenburg JJ, Hendrikse J, van der Kolk AG, Luijten PR, Biessels GJ. High resolution imaging of cerebral small vessel disease with 7T MRI. Acta Neurochir Suppl 2014; 119: 125–30.

van Veluw SJ, Zwanenburg JJ, Rozemuller AJ, Luijten PR, Spliet WG, Biessels GJ. The spectrum of MR detectable cortical microinfarcts: a classification study with 7-tesla postmortem MRI and histopathology. J Cereb Blood Flow Metab 2015a; 35: 676–83.

van Veluw SJ, Hilal S, Kuijf HJ, Ikram MK, Xin X, Yeow TB, et al. Cortical microinfarcts on 3T MRI: clinical correlates in memory-clinic patients. Alzheimers Dement 2015b; 11: 1500–9.

van Veluw SJ, Biessels GJ, Luijten PR, Zwanenburg JJ. Assessing cortical cerebral microinfarcts on high resolution MR images. J Vis Exp 2015c; 105.

van Veluw SJ, Biessels GJ, Klijn CJ, Rozemuller AJ. Heterogeneous histopathology of cortical microbleeds in cerebral amyloid angiopathy. Neurology 2016; 86: 867–71.

Vonsattel JP, Myers RH, Hedley-Whyte ET, Ropper AH, Bird ED, Richardson EP Jr. Cerebral amyloid angiopathy without and with cerebral hemorrhages: a comparitive histological study. Ann Neurol 1991; 30: 637–49.

Wardlaw JM, Smith EE, Biessels GJ, Cordonnier C, Fazekas F, Frayne R, et al. Neuroimaging standards for research into small vessel disease and its contribution to ageing and neurodegeneration. Lancet Neurol 2013; 12: 822–38.